

## Irradiation of thorium-bearing molten fluoride salt in graphite crucibles

Hania, P. R.; Boomstra, D. A.; Benes, O.; de Koning, A. J.; de Groot, S.; Konings, R. J.M.; Capelli, E.; Baas, P. J.; Lippens, G. I.A.; More Authors

**DOI**

[10.1016/j.nucengdes.2021.111094](https://doi.org/10.1016/j.nucengdes.2021.111094)

**Publication date**

2021

**Document Version**

Final published version

**Published in**

Nuclear Engineering and Design

**Citation (APA)**

Hania, P. R., Boomstra, D. A., Benes, O., de Koning, A. J., de Groot, S., Konings, R. J. M., Capelli, E., Baas, P. J., Lippens, G. I. A., & More Authors (2021). Irradiation of thorium-bearing molten fluoride salt in graphite crucibles. *Nuclear Engineering and Design*, 375, Article 111094. <https://doi.org/10.1016/j.nucengdes.2021.111094>

**Important note**

To cite this publication, please use the final published version (if applicable). Please check the document version above.

**Copyright**

Other than for strictly personal use, it is not permitted to download, forward or distribute the text or part of it, without the consent of the author(s) and/or copyright holder(s), unless the work is under an open content license such as Creative Commons.

**Takedown policy**

Please contact us and provide details if you believe this document breaches copyrights. We will remove access to the work immediately and investigate your claim.



# Irradiation of thorium-bearing molten fluoride salt in graphite crucibles

P.R. Hania<sup>a,\*</sup>, D.A. Boomstra<sup>a</sup>, O. Benes<sup>b</sup>, P. Soucek<sup>b</sup>, A.J. de Koning<sup>a</sup>, I. Bobeldijk<sup>a</sup>,  
S. de Groot<sup>a</sup>, R.J.M. Konings<sup>b</sup>, E. Capelli<sup>b,c,1</sup>, M. Naji<sup>b</sup>, C. Sciolla<sup>a</sup>, P.J. Baas<sup>a</sup>,  
V. Bhimanadam<sup>a</sup>, N.B. Siccama<sup>a</sup>, G.I.A. Lippens<sup>a</sup>

<sup>a</sup> Nuclear Research & Consultancy Group (NRG), Westerduinweg 3, NL-1755LE Petten, The Netherlands

<sup>b</sup> European Commission Joint Research Center (JRC), Hermann-von-Helmholtz Platz 1, D-76125 Karlsruhe, Germany

<sup>c</sup> Delft University of Technology, Mekelweg 15, NL-2629JB Delft, The Netherlands

## ARTICLE INFO

### Keywords:

Molten salt  
Fuel  
Fission product behaviour  
MTR irradiation  
Design

## ABSTRACT

Four fluoride fuel salt samples ( $78\text{LiF}\cdot 22\text{ThF}_4$ ) in graphite crucibles were irradiated in the HFR Petten for a duration of 508 Full Power Days under the name SALIENT-01 (SALT Irradiation Experiment). Goal of the experiment was to gain experience with the design of liquid salt experiments and the handling of the salts before and after irradiation. Specific research goals for SALIENT-01 are (i) to confirm claims of good fission product retention in the salt, (ii) to obtain size distributions for noble metal particles using Transmission Electron Microscopy and (iii) to assess possible interactions between fuel salt and fine-grained nuclear graphite, as well as possible uptake of fission products by the graphite. Here the design and irradiation history of the experiment are discussed together with plans for post-irradiation examinations. Limitations in representativeness of this experiment and capsule irradiations in general are discussed as well as follow-up actions to improve the quality of future irradiations.

## 1. Introduction

The Molten Salt Reactor (MSR) is a high-potential technology for sustainable and safe nuclear energy production that has received growing interest in the past 10 years (LeBlanc, 2010; Serp et al., 2014). The technology has been recognized by the Gen-IV International Forum through the reactor concepts of the Molten Salt Fast Reactor (MSFR), developed mainly in the EU, and the Fluoride-cooled High temperature Reactor (FHR) mainly developed in the US and China (Serp et al., 2014; Merle et al., 2008). An older, well-known and publically available design is the thermal Molten Salt thorium Breeder Reactor (MSBR), developed by the US Oak Ridge National Laboratory (ORNL) in the 1960s and early 70s (Robertson, 1971; Rosenthal, 1972). The graphite-moderated, fluoride salt fueled MSR concept is currently developed by SINAP in China and in the US by FLIBE Energy under the name Liquid Fluoride Thorium Reactor (LFTR), while Terrestrial Energy (Canada) develops a more simple and compact, uranium-based MSR design to reduce time to market.

The flexible MSR concept allows for a multitude of initiatives and ideas, such as a waste burner for nuclear waste reduction options, fast-

spectrum uranium-plutonium (chloride) breeders, and the introduction of a thorium nuclear fuel cycle. These ideas build on the strong advantages of liquid salt as a carrier for fissile and fertile isotopes over conventional solid fuel: operation at essentially ambient pressure, absence of damage accumulation of the fuel salt under neutron irradiation, absence of traditional ‘loss of coolant’ accidents, passive avoidance of core melt by flushing the fuel-coolant combination to a high surface area decay tank, a strongly negative core reactivity coefficient resulting from thermal expansion of the salt, and the possibility of on-line salt processing to improve neutron economy and reduce activity in the core. These benefits should in principle result in safer, reduced-cost operation.

Similar to other advanced reactor concepts however, the MSR faces significant challenges in the area of fuel and material qualification through a combination of high temperature of operation, a corrosive environment and intense neutron irradiation. In the area of construction materials, the route to qualification will likely involve prolonged exposure to an environment combining high temperature, neutron fluence and flowing salt (Zheng et al., 2016; Sabharwall et al., 2010; Carpenter et al., 2017); on-line management of salt (redox) chemistry will

\* Corresponding author.

E-mail address: [hania@nrg.eu](mailto:hania@nrg.eu) (P.R. Hania).

<sup>1</sup> Currently at Orano, 125, Avenue de Paris 92320, Châtillon, France.

be required to reduce its corrosive action on containment materials (Olson, 2009; Kelleher, 2015; Alekseev and Shimkevich, 2016; Gibilaro et al., 2015); the behavior of fission products under accident conditions should be charted to obtain credible source terms (Benes and Konings, 2013; Taira et al., 2017); and tritium production and diffusion forms an additional challenge if a lithium salt is used (Carpenter et al., 2017; Forsberg et al., 2017).

Recognizing both the high potential of MSR technology and the need to perform in-pile experiments for material qualification and objective safety evaluations, NRG together with JRC Karlsruhe has set out to perform a series of molten fuel salt irradiations in the High Flux Reactor (HFR) in Petten, The Netherlands. The goal is to establish irradiation experience as well as experience with the design of molten salt samples, the handling of irradiated salt and the treatment of salt waste produced by these irradiations. Similar work on fuel-free coolant salt has been carried out in the US by MIT in the framework of the FHR (Zheng et al., 2016; Carpenter et al., 2017). Main topics to be investigated are fission product speciation and relocation, in-pile corrosion and materials aging, and salt reprocessing. The intention is to gradually increase the complexity of the irradiations in the form of salt buffering, redox control, fission gas removal through helium bubbling, and salt flow. The introduction of salt flow may be realized at NRG by introducing a closed, pumped fuel salt loop in the HFR reactor pool with the 'hot leg' adjacent to the reactor vessel (Stempniewicz, et al., 2017).

As a first step, an irradiation of four small  $78\text{LiF}\text{-}22\text{ThF}_4$  samples in graphite crucibles has been conducted under the name SALIENT-01 (SALt Irradiation Experiment). The  $78\text{LiF}\text{-}22\text{ThF}_4$  eutectic composition is the currently adopted starting point for MSFR fuel and blanket salt; this particular composition does not initially contain fissile material, but fission power is built up over the course of months through breeding of U-233. Graphite as the default moderator material for thermal MSR designs is well compatible with molten fluoride salts (Grimes, 1963a; Toth and Gilpatrick, 1972). The specific goals for SALIENT-01 are to confirm claims of high fission product stability in the salt through post-irradiation Knudsen-cell effusion mass spectrometry (KEMS) tests, in particular with respect to Cs and I which dominated the release of activity during conventional reactor accidents such as the Fukushima accident; to measure fission gas release; to obtain size distributions for noble metal particles; and to assess possible interactions between fuel salt and fine-grained nuclear graphite, as well as possible uptake of fission products by the graphite.

The SALIENT-01 irradiation has run from August 2017 to August 2019 for a total duration of 508 full power days, divided over 17 cycles of around 30 days with varying downtime in between cycles. This paper treats sample preparation, the design of the experiment and experimental feedback from the irradiation period. Challenges encountered in the design phase and limitations in representativeness of capsule irradiations in general are discussed, as well as follow-up actions to improve the quality of future irradiations.

## 2. Sample preparation

### 2.1. Synthesis of salt samples

The  $\text{LiF}\text{-ThF}_4$  eutectic (composition  $78\text{LiF}\text{-}22\text{ThF}_4$ ) was produced at JRC Karlsruhe by direct mixing of the end members at the following mass ratio:  $m(^7\text{LiF}) = 6.6031\text{ g}$ ,  $m(\text{ThF}_4) = 22.0074\text{ g}$ .  $^7\text{LiF}$  was produced from commercially obtained  $^7\text{LiOH}$  (99.9%  $^7\text{Li}$  enrichment) by HF treatment in aqueous solution until neutral pH was observed. The formed  $\text{LiF}$  precipitated from the solution in the form of small particles which were separated by vacuum filtration. The obtained powder was successively pre-dried under air at  $200\text{ }^\circ\text{C}$  for 2 h to loose most of the moisture and yet dried under argon at  $350\text{ }^\circ\text{C}$  for 4 h to obtain moisture-free  $\text{LiF}$ . The full process of converting  $\text{LiOH}$  to  $\text{LiF}$  yielded 92% of theoretical quantity.  $\text{ThF}_4$ , on the other hand, was produced by gaseous hydrofluorination from low-fired (high surface)  $\text{ThO}_2$  powder as

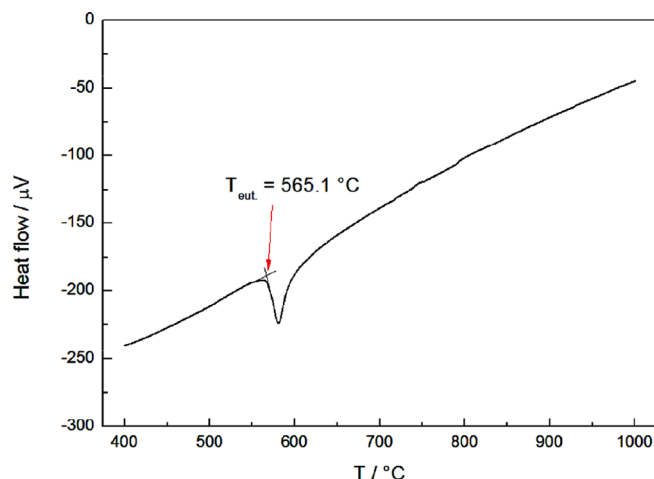


Fig. 1. DSC analysis of the  $78\text{LiF}\text{-}22\text{ThF}_4$  composition showing a eutectic composition measured at  $565.1\text{ }^\circ\text{C}$ .



Fig. 2. Exploded view of crucible (diameter  $\sim 22\text{ mm}$ , length  $80\text{ mm}$ ), showing from left to right: the crucible, the salt column, 3 activation monitor sets, the end cap, a metallic filter prepared from a stack of stainless steel wire meshes, and the filter cap. The crucible walls contain additional holes for thermocouples and gas lines.

described in ref. (Souček et al., 2017). Both synthesized end-members were tested on purity, applying two methods: (i) XRD for phase analysis and (ii) DSC for melting point determination. The combination of both techniques has been demonstrated as a reliable method for purity analysis (Souček et al., 2017) and no impurities were detected in the present case. Oxygen impurities at the ppm-level can however not be ruled out.

The end-members have been put together in a plastic bottle and shaken for five minutes. Such mixture was afterwards homogenized in an agate mortar to achieve fine powder which was checked by DSC for melting temperature revealing only one equilibrium point, indicating a eutectic composition found at temperature  $565.1\text{ }^\circ\text{C}$  (Fig. 1), in good agreement to previous data ( $568\text{ }^\circ\text{C}$  Benes and Konings, 2012).

### 2.2. Preparation and filling of the crucibles

Fig. 2 gives an impression of a graphite crucible and its contents, while Table 1 summarizes relevant information on the five irradiated crucibles, numbered L1-L5 from bottom to top in the SALIENT-01 sample holder. High-density fine-grained graphite from two different manufacturers have been used: PCIB graphite from Graftech, and T950 from Sinosteel. The behaviour of PCIB graphite under irradiation has been thoroughly characterized in NRG's INNOGRAPH irradiation experiment (Heijna et al., 2017; Vreeling et al., 2008). Sinosteel's T950

**Table 1**  
Summary of samples.

Crucible nr. (bottom to top)	Graphite type	Sample weight (g)	Th-232 wt (g)	Column height* (mm)	Salt column diameter (mm)	Notes
L1	PCIB	7.1293	4.1331	36.4	7.6	Ni-201 foam
L2	T-950	6.1344	3.5564	36.4	7.0	
L3	PCIB	6.2791	3.6403	36.6	7.0	
L4	T-950	7.1743	4.1592	37.1	7.8	0.1 mm Ni-201 foil contains 316 SS tube
L5	PCIB	–	–	–	–	

\* Determined at room temperature.



**Fig. 3.** Crucible loading at JRC Karlsruhe (top left: loading of the LiF-ThF<sub>4</sub> powder mixture, top right: same crucible after melting), and assembly of sample holder at NRG (bottom).

was found to be similar to PCIB in terms of density (1.857 g/cm<sup>3</sup> for PCIB against 1.832 g/cm<sup>3</sup> for T950), apparent porosity (11.7% for PCIB against 15.8% for T950) and microstructure. Following metrology and checks for defects using X-ray tomography, the crucibles were cleaned ultrasonically in methanol and distilled water, then dried for 4 h in air at 100 °C and subsequently for 8 h at 1000 °C in argon. The procedure was taken from Olson (Olson, 2009) and was performed to keep the graphite free from moisture and thereby reducing the chance of contaminating the salt and of failure of the thermocouples placed in the graphite during assembly. The graphite lids containing a stack of stainless steel mesh (gauze) filters (316SS, BS-410 mesh 300) have been treated using the same procedure, except for the last drying step during which the temperature was kept at 500 °C to avoid damage to the metallic parts. One of the salt-carrying crucibles (L4) carries a 100 µm nickel-201 foil lining the inner wall, leaving sufficient space circumferentially to accommodate graphite shrinkage. This foil was added to allow for a comparison of noble metal deposition on graphite and metal. The foil was etched in nitric acid to remove the oxygen skin. Similarly, a small piece of high surface area nickel foam (American Elements, 99.99% purity, porosity >95.1%) is located at the bottom of crucible L1. Crucible L5 containing a

short 316 stainless steel tube was added to the sample matrix as a reference heated only by nuclear heating (mostly gamma heating).

The powder mixture of the LiF-ThF<sub>4</sub> composition was poured into the dried graphite crucibles under argon atmosphere in five steps, each one consisting of densification in the solid state using a stainless steel piston fitting exactly the dimensions of the crucible interior (Fig. 3). At each step the salt was brought to a molten state at 650 °C for 30 min (under Ar atmosphere of c(O<sub>2</sub>) and c(H<sub>2</sub>O) < 1 ppm) with heating and cooling ramps of 10 K/min, resp. 5 K/min. Each melting procedure decreased the salt volume by factor of around 2.5. It was observed that during each heat pre-melting step the weight loss of the crucible was negligible compared to the total amount of the salt. The color of the salt after final melting was white with black particles on the top, which have been identified as graphite traces; this is a typical observation when melting fluoride salts in graphite containers.

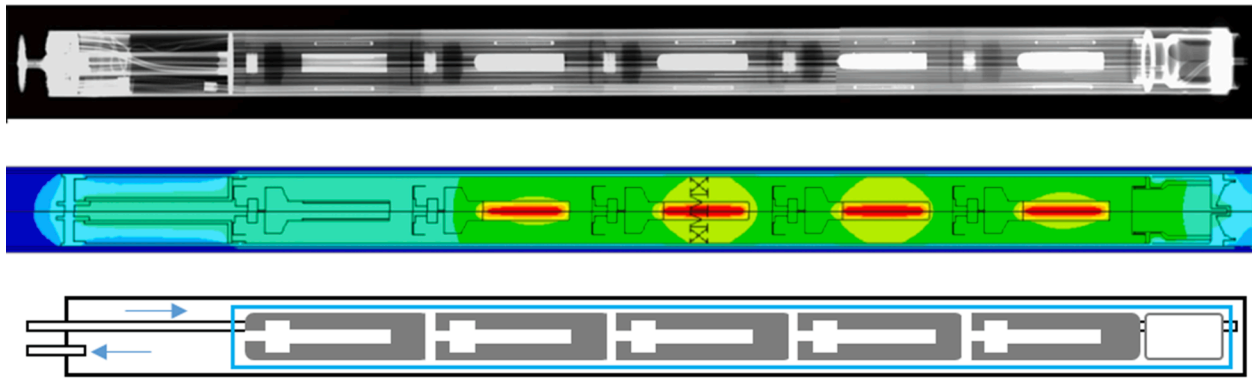


Fig. 4. The SALIENT-01 sample holder (from bottom to top: a sketch showing the 1st (blue, sealed) and 2nd (black, flushed with inert gas) containments, the finite element model used for temperature calculations, and an X-ray image for quality control after fabrication). (For interpretation of the references to color in this figure legend, the reader is referred to the web version of this article.)

### 3. Design and fabrication of the irradiation facility

#### 3.1. Irradiation parameters

A sample burn-up of 1.5 – 2% FIHMA is targeted as a compromise between irradiation duration and the need to determine post-irradiation high-temperature Cs release rates from these samples using Knudsen Cell effusion. A burn-up of 1% FIHMA was previously demonstrated to be sufficient for carrying out such high-temperature Cs release tests when performed on  $\text{UO}_2$  fuel.

As a design requirement, salt temperatures during irradiation should be above the melting point (568 °C (Beneš and Konings, 2012)) and not become higher than 1200 °C under any foreseeable circumstances; the latter is still more than 500 °C below the boiling point (1760 °C (Beneš and Konings, 2012)), which avoids high vapour pressures. Target temperature for the crucible walls was set at around 50 °C above the melting temperature. The temperature distribution in the salt should furthermore be determined accurately with regards to interpretation of post-irradiation examinations.

#### 3.2. Description of sample holder

The stack of 5 graphite crucibles as described above is irradiated in a 321 stainless steel sample holder occupying a dry channel with a diameter of 31 mm; the channel walls are water-cooled thereby providing a heat sink. The sample holder is connected to a vertical displacement unit (VDU) in the head of the TRIO facility, which allows for vertical movement of the sample holder to adjust its position with respect to the HFR flux profile.

The sample holder itself provides double containment, while a third containment is provided by the dry channel (which is part of a larger standard TRIO-facility). The first containment of the sample holder (as indicated in Fig. 4, bottom) is filled with a 70%Ne-30%He gas mixture (Ne6.0/He6.0) at 1 bar(a) (20 °C) providing suitable thermal isolation. Since fluoride salts easily pick up moisture and can react with oxygen, the first containment was thoroughly dried with flowing helium at 120 °C for 48 h while checking for humidity before filling with the helium-neon mixture and sealing by welding. The volume of the sealed gas plenum in the first containment (81 cm<sup>3</sup>) was chosen such that the expected combined fission gas release from the 4 open salt-carrying crucibles can be measured by post-irradiation puncture of the first containment followed by mass spectrometry. Pressures in the second and third containment are measured during irradiation to monitor the integrity of the first, second and third containment. The composition of gas mixtures (He/Ne/N<sub>2</sub>) in the second and third containment can be adjusted during irradiation by flushing to allow temperature control; this also allows monitoring of activity in the 2nd and 3rd containments

through the outflowing gas.

To confirm estimated burn-up after irradiation, each graphite crucible is equipped with 3 activation monitor sets containing Ni-Co, Fe, Ti and Nb activation materials at a single axial position and 120° relative angles in the horizontal plane (Fig. 2). In addition, 18 thermocouples (type K, MgO insulation, 316SS sheath, 1 mm, ThermoCoax) in the walls of the 5 graphite crucibles monitor the graphite wall temperature during irradiation. The thermocouples are placed 18 mm above the bottom of the salt column, which is at the vertical centerline of the salt columns. Calibrated burn-up calculations will be performed based on measured material activations from the monitor sets and the irradiation history of the samples. Computational Fluid Dynamic (CFD) simulations can then be performed using the obtained power history of the salt and the in-pile measurement of crucible temperature. These simulations will provide an estimate of the temperature distribution in the salt as a function of time.

#### 3.3. Nuclear analysis

Supporting nuclear calculations were performed by means of the MCNP4C3 code (MCNP, 2000). Starting point is a detailed MCNP model of the HFR core. This model was combined with a detailed model of the SALIENT-01 sample holder. Nuclear data were taken from JEF-2.2 for <sup>27</sup>Al and <sup>235</sup>U, and from ENDF/B-VI.5 for all other nuclides. The combination of the MCNP4C3 code with these nuclear data has been validated using several benchmark cases as well as dedicated validation studies. Unless otherwise specified, for all the results discussed here the statistical uncertainty is less than 2% (1σ). Evolution of sample composition was simulated using the OCTOPUS script, which invokes MCNP and FISPACT calculations in a leap-frog manner. The irradiation was simulated as a number of 90-day intervals, each followed by a 30 days cooling interval. This was done to clarify the effects of downtime (notably <sup>233</sup>Pa decay) on fuel power. The total irradiation time targeted was > 500 (max. 540) effective full-power days.

Main outputs of these calculations are the fuel power as a function of irradiation time, the leg-averaged nuclear heating in W/g as a function of vertical position (applied in thermomechanical analysis to all materials except the fuel salt), neutron damage in the graphite, activation of construction materials and finally the nuclide inventory in the salt as a function of time. Peak nuclear heating in the SALIENT-01 facility is around 4.5 W/g in HFR in-core position G3/G7 and 3.3 W/g in HFR in-core H4. Damage to the crucible graphite ranges from 5 to 7 dpa at the end of irradiation in position HFR in-core G3/G7; the post-irradiation calculations will yield slightly lower values due to the move to position H4. The same holds for thermal (<0.625 eV) and Fast (0.082–1.96 MeV) flux levels, which are  $5.9 \times 10^{13} \text{ cm}^{-2}\text{s}^{-1}$  and  $7.2 \times 10^{13}$  respectively in G3/G7 (Center Line Core ± 300 mm).

The total sample-average nuclear power (photon and neutron

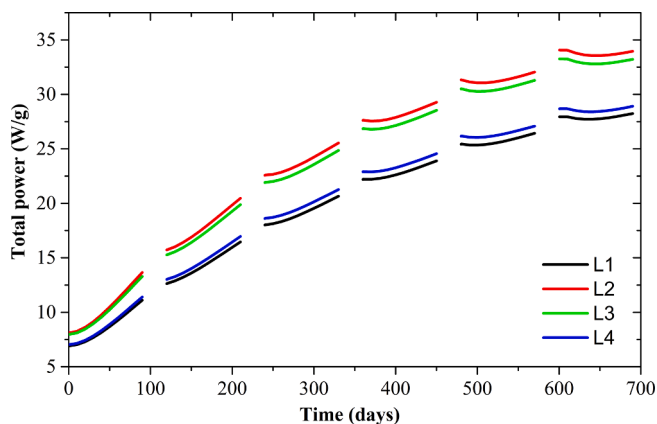


**Fig. 5.** Total power in W/g vs. ‘irradiation days’ in samples L1-L4, for irradiation in HFR in-core position G7 N/W (top) and in H6 S/W (bottom). The X-axis includes artificial periods of reactor operation of 90 days followed by ‘shutdown times’ of 30 days. This artificial irradiation history was chosen to specifically include effects of long reactor stops.

contributions, fission included) as a function of irradiation time is shown in Fig. 3 for HFR in-core position G3/G7. At the start of irradiation the power in the samples is similar to the nuclear heating (~4.5 W/g) in the surrounding materials, but production of fissionable U-233 slowly leads to an increase in fuel power towards the end of irradiation. The increased fuel power following 30-day reactor downtime are also clearly visible; actual downtime in between HFR cycles is expected to be between 4 and 18 days. In HFR in-core position H4/H6 the fuel power at end of irradiation is not expected to exceed 30 W/g.

Fuel burn-up at end of irradiation calculated for HFR in-core position G3/G7 is 1.8% FIHMA. Maximum pressure build-up in the 1st containment from fission gas production is 0.24 bar (20 °C) at full release; initial pressure is 1.0 bar (20 °C).

Tritium production by the experiment was calculated to assess whether some form of active tritium management was needed. Tritium production in SALIENT-01 is suppressed by using Li-7 enriched to 99.9%. The total production during a 540 FPD (Full Power Day) irradiation in HFR in-core position G3/G7 is ~ 40 μmol/cm<sup>3</sup> salt or ~ 280 GBq for the SALIENT-01 experiment (containing around 7 cm<sup>3</sup> of salt) over the entire duration of irradiation. Burn-up calculations show that the build-up of tritium is close to linear. The inferred 14 GBq of tritium per cycle is in the same order of magnitude as overall tritium production

in the HFR core. It was concluded that even in case of full tritium release from SALIENT-01 to the reactor basin, the total release stayed well within allowed values.

### 3.4. Thermo-mechanic and salt flow analysis

Finite Element Method (FEM) computations were performed in order to determine the gas gap widths and gas mixture changes needed to keep the crucibles at constant temperature under increasing power generation (Fig. 5) in the salt, and to evaluate thermal stress in the containment structures. The analysis was performed using the general FE code ANSYS (v15.0). An axial 2-D model was set up with element type PLANE223 (2-D 8-Node Coupled-Field Solid) with the respective key options set to structural-thermal and plane stress. The axially symmetrical model does not contain details on the thermocouples and monitor sets; the effects of the thermocouples in the crucible walls were instead explored separately in a radial 2-D model of the sample holder. The main effect, caused by lower effective thermal conductivity and the higher density of the thermocouples, was found to be a temperature increase of the crucibles of +18 °C, consistently for all load cases.

FEM computations confirmed that constant graphite wall temperature in the range 580–630 °C can be ensured by using N<sub>2</sub>-Ne mixtures at the beginning of irradiation and gradually moving to Ne-He mixtures towards the end of irradiation (i.e. at higher fuel power density). The effect of graphite shrinkage, which will cause the gap between crucible wall and 1st containment to widen, was evaluated as well (it was not needed to account for swelling given the calculated accumulation of damage in the graphite of <7 dpa (Heijna et al., 2017; Vreeling et al., 2008). For nuclear grade PCIB graphite, known shrinkage is 2 vol-% (Heijna et al., 2017), while no data is available for the T-950 graphite from Sinosteel. However, considering the range of values obtained for different graphites in the Innograph experiment (Heijna et al., 2017), a maximum shrinkage of 5 vol-% (or 1.64% in any one dimension) was assumed. The outer diameter of the graphite crucibles was therefore reduced from 26.0 to 25.6 mm to model the effect of graphite shrinkage (note that this case is conservative in that the shrinkage of the inner diameter and therefore the linear heat rate for the salt samples has not been taken into account). This produced a temperature increase of the crucible walls up to 80 °C at maximum fuel power, which could be compensated by change of gas mixture in the inter-containment gaps.

A stress analysis was performed for both the 1st and 2nd containment. The maximum first containment temperature and stress were checked against ASME III nuclear safety standards (ASME, 2010). The ‘worst case’ with respect to stress levels was found to be the case of high

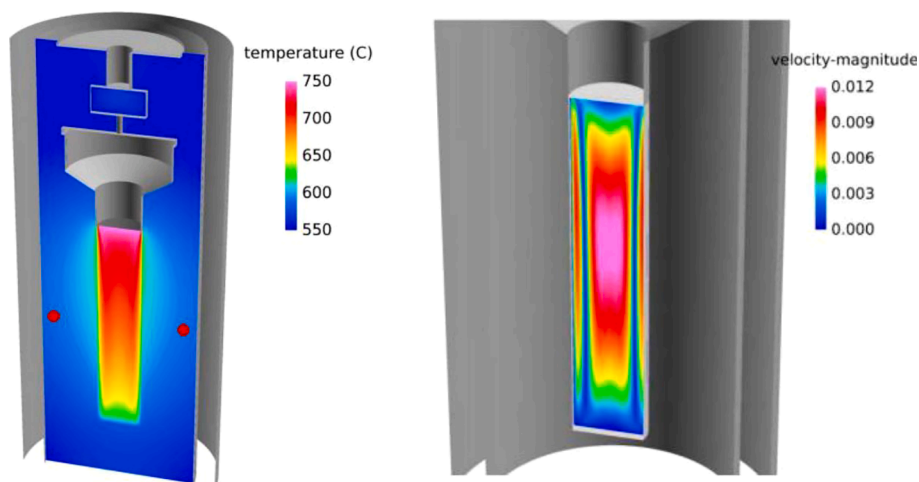


**Fig. 6.** Results of CFD analysis for crucibles 1 and 4, at 23 W/g assumed salt power (corresponding roughly to the power at end of irradiation) and thermocouple temperatures of 590 °C. (Left) temperature distribution in the salt and graphite in °C; approximate thermocouple positions are indicated by red dots. (Right) salt velocity magnitude in m/s. (For interpretation of the references to color in this figure legend, the reader is referred to the web version of this article.)

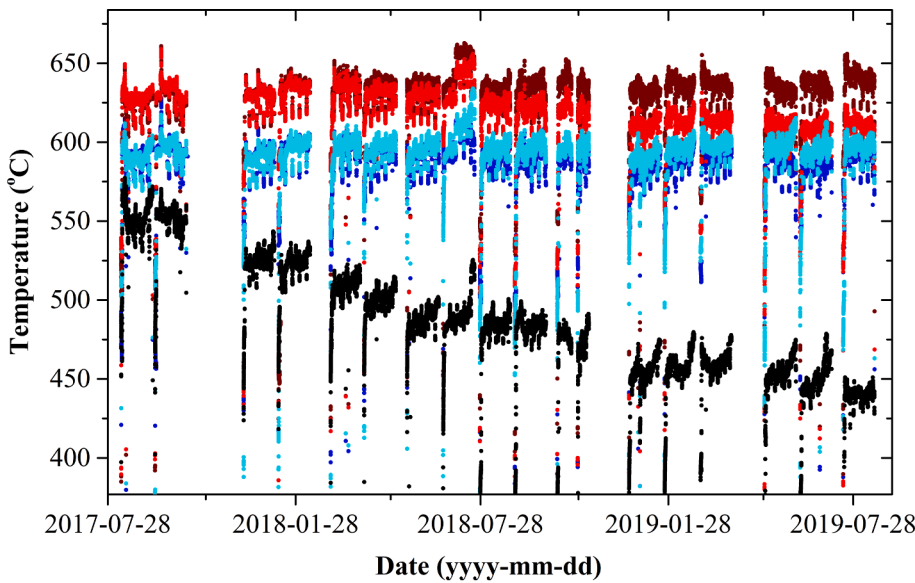
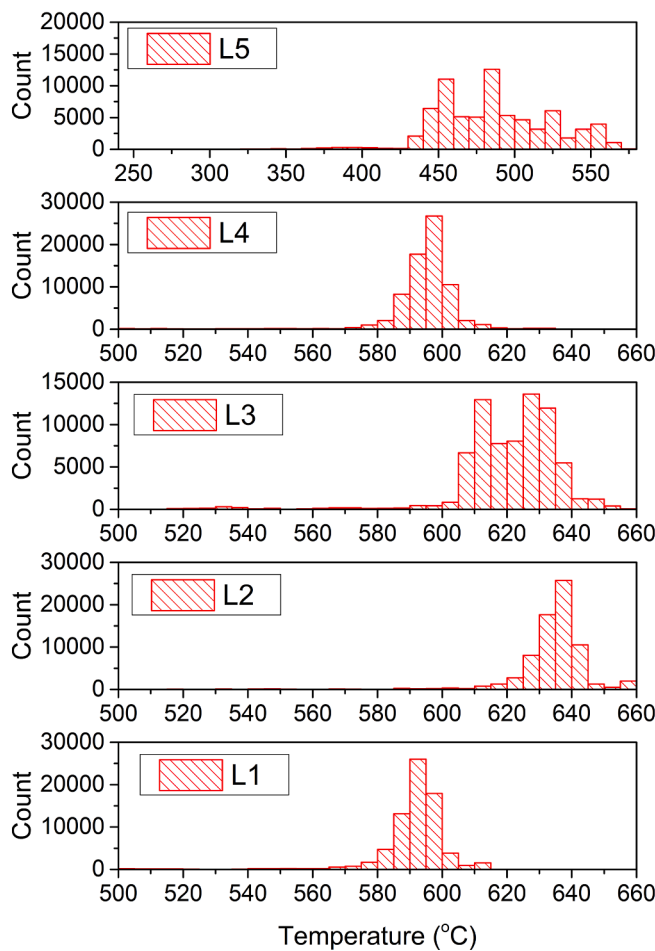


**Fig. 7.** (top) Wall temperatures for for crucibles L1 (dark blue), L2 (dark red), L3 (bright red), L4 (light blue) and L5 (black). Averages are over the 3–4 thermocouples in a capsule; for thermocouple positions see Fig. 6. The observed small (~20 °C) temperature jumps are related to changes in the HFR core configuration (mostly the insertion/removal of isotope production targets). (bottom) Associated temperature histograms for the 5 crucibles. (For interpretation of the references to color in this figure legend, the reader is referred to the web version of this article.)



nuclear heating combined with low temperature (i.e. 100% helium in the 2nd and 3rd containment), and the highest stress was located in the containment bottom. Assuming a pressure of 50 bar in the 1st containment, no stress intensities above the allowable limits are obtained for N<sub>2</sub>/Ne mixtures in HFR in-core position G7 and for any gas mixtures in HFR in-core position H6. Therefore, the use of helium was not permitted in HFR in-core position G7 in order to stay within the ASME allowed

parameter space. The containment temperature remains below the creep temperature of 316 stainless steel under all operation conditions.

Two- and three-dimensional CFD simulations have been performed using Fluent version 15 to obtain information on the temperature distribution in the salt and on its flow pattern. Ref. (Beneš and Konings, 2012) was used for the properties of the LiF-ThF<sub>4</sub> eutectic salt. Gravity was included in the model. The salt flow is laminar and steady-state.

Fig. 6 shows the temperature distribution (left) and liquid velocity (right) in the salt of crucibles 1 and 4 at a fuel specific power of 23 W/g and thermocouple temperatures of 590 °C. Additional simulations have been performed, screening for sensitivity to uncertainties in salt viscosity (up to 2× higher compared to ref. (Beneš and Konings, 2012) and thermal conductivity (1–1.5/mK). The simulations confirm that the minimum and maximum salt temperature, the maximum filter temperature, the maximum salt velocity and maximum shear stress can be estimated with reasonable accuracy as a function of thermocouple temperature and total power produced in the salt. Based on these simulations and measured spread in in-pile thermocouple temperatures, the salt temperature in SALIENT-01 is expected not to exceed 850 °C. The variation of the temperature at the surface of the crucible stays within 40 °C. Hot salt with a lower density is flowing upward in the center with a speed of  $12 \pm 1$  mm/s. Near the walls, the salt cools down resulting in a higher density, flowing downward with approximately the same velocity. The flow of salt gives a maximum shear stress of  $0.4 \pm 0.08$  Pa on the inner surface of the crucible. These values are two orders of magnitude below those for salt flowing through piping at a speed of a few m/s.

### 3.5. Consideration of room temperature radiolysis in SALIENT-01 design

A specific concern during the design phase was the possible production of fluorine gas through radiolysis as reported previously by ORNL (Haubenreich, 1970; Toth and Felker, 1990; Williams et al., 1996). Since the SALIENT-01 design does not include electric heating, the salt samples cool down to near room temperature (50–60 °C) during HFR shutdown periods. In normal circumstances these shutdown periods vary from 5 to 18 days in length, and during this time SALIENT-01 is stored in an “experiment rack” in the reactor pool.

Several reports from Oak Ridge National Lab have described the issue of radiolytic production of fluorine gas at salt temperatures below 70–150 °C (Haubenreich, 1970; Toth and Felker, 1990; Williams et al., 1996; Grimes, 1963b, 1964, 1965), and the subsequent high-temperature reaction between the generated fluorine gas and the materials in its surroundings. In addition, Williams et al. (1996) summarize results from different beam irradiations of fresh fluoride salts, while Toth and Felker (1990) discuss a limit to fluorine loss from MSRE salt as well as a measurement of the activation energy for the strongly temperature-dependent reverse reaction (see the Appendix at the end of this paper). The issue is also touched on in a recent article by Forsberg and Peterson on FHR spent fuel issues (Forsberg and Peterson, 2015).

As obtained from these sources, the radiolytic fluorine gas production is driven by absorption of on the one hand the gamma field that is part of the decay heat from the material test reactor and on the other hand decay heat (alpha, beta and gamma radiation) in the sample itself; ionizing radiation produced by the surrounding graphite is <1% of that of the salt itself, and this contribution can be neglected. The absorption of radiation in the fuel salt breaks chemical bonds in the salt, supposedly producing atomic fluorine which diffuses to open surfaces where F<sub>2</sub> molecules are formed. The reverse reaction, recombination of atomic fluorine with lattice defects, depends strongly on temperature and becomes dominant above 70–150 °C. At ambient temperatures the combination of radiolytic bond cleavage, diffusion of fluorine and recombination with lattice defects leads to a net liberation of F<sub>2</sub>(g) from the salt.

Fluorine gas production and possible impact on experiment safety were reviewed in the context of safety evaluation; a discussion is attached at the end of this paper as an appendix.

## 4. Irradiation

The SALIENT-01 irradiation was started on August 10, 2017 and finished on August 17, 2019, for a total irradiation time of 508 effective full power days. Feedback from the thermocouples in the graphite crucible walls confirmed that the correlation between crucible wall

temperatures and gas mixtures in the 2nd and 3rd containment was correctly modeled in the design phase (nuclear and thermo-mechanic analysis).

Fig. 7 (top) gives the crucible wall temperatures for the four salt-filled crucibles (L1-L4) and the dummy (L5) containing only the 316 steel piece, and Fig. 7 (bottom) the associated temperature histograms. Average wall temperatures over the course of irradiation were 591 and 594 °C for crucibles L1 and L4, and 633 and 621 °C for the centrally located crucibles L2 and L3. The wall temperatures of crucibles L1-L4 were actively kept from increasing due to the predicted fission power increase by changing gas mixtures in the surrounding gas gaps, as can be seen in the figure, which clearly shows a decreasing temperature for the dummy crucible.

Several SCRAM events have occurred during the irradiation of SALIENT-01, all of which were unrelated to the experiment. During these SCRAM events the crucible wall temperature never went below 90 °C. However, in between irradiation cycles, the samples cooled down relatively quickly to below 70 °C for periods varying between 4 and 30 days, which may have resulted in the production of fluorine gas. If fluorine was indeed formed in the ‘cold’ periods in between irradiation cycles, exothermic reactions of the fluorine with the graphite crucibles or the steel containment could result in small spikes in the recorded temperature during the start-up phase of the following cycle (see Section 3.5). Temperature excursions were not observed however during any start-up phase, indicating that fluorine gas generation was limited. Because of the possibility of fluorine corrosion of the 1st containment, attention was also paid to possible activity increases in the 2nd containment. No irregular increased activity was however observed in the 2nd containment, allowing to conclude that the 1st containment remained intact throughout the irradiation.

Due to the increasing power density in the salt samples and the limitations to temperature compensation, the experiment was transferred from its original position (G7) to a slightly lower flux position (H4) after 8 cycles of operation. Fig. 7 (top) shows indeed that the crucible wall temperatures are somewhat elevated in the 8th cycle, an issue caused by temporary malfunction of the vertical displacement unit.

## 5. PIE program and waste treatment

### 5.1. Post-irradiation examinations

After a required cooling period, the sample holder was transported on-site to NRGs Hot Cell Laboratories for post-irradiation examinations. Following removal of the 2nd containment, the 1st containment will be punctured for gas analysis by mass spectrometry; this will yield data on fractional fission gas release and possibly yield an indication of fluorine gas production (F<sub>2</sub>(g) and/or CF<sub>4</sub>(g)).

The 1st containment will be opened inside an alpha-tight hot-cell for visual inspection of the inside of the containment and the graphite crucibles. Extensive Optical and Electron Microscopy (SEM) will then be performed on the graphite surfaces, metal filters and foils, bulk salt, fuel-graphite interface and bulk graphite. This should yield information on fission product penetration into the graphite, noble metal particle size, relocation of volatile fission products and the extent of fluorine corrosion. At least one salt sample will be stored in an airtight container with a pressure sensor to study long-term fluorine gas release behavior.

Small salt samples will be sent to JRC Karlsruhe for Knudsen Cell Effusion tests. In these tests the samples will be subjected to a temperature ramp to complete evaporation, which should yield information on the high-temperature stability of fission products (and in particular Cs) in the irradiated salt. Furthermore, Transmission Electron Microscopy will be used to observe 5-metal particle precipitates and to determine their size distribution.

Final evaluation of maximum salt temperatures and burn-up will be performed in the post-irradiation examination phase. Calibrated MCNP/FISPACT calculations will first be performed on the basis of monitor set

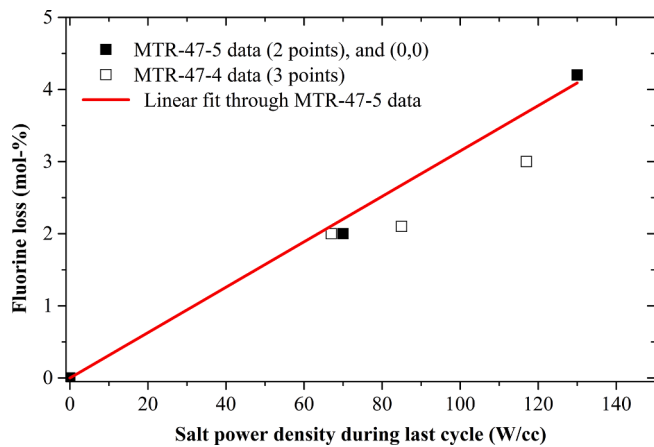


**Fig. 8.** Linear dependence between salt power density before shutdown and post-irradiation fluorine loss for MSRE salt, inferred from experiment MTR-47-5. 3 additional data points were reported for experiment MTR-47-4, but these were not used in the fit since for this experiment only the average power densities are given (Grimes, 1964, 1965).

activations to obtain salt powers and burn-up. These results will then be used as input for CFD calculations evaluating salt flow and temperature distributions.

### 5.2. Interim storage and waste treatment

Since the SALIENT-01 irradiation and possible follow-up experiments produce chemically exotic high-level waste, it is essential to secure waste routes and suitable waste forms. In The Netherlands, radioactive waste from different sources is collected by the Central Organization for Radioactive Waste (COVRA) for treatment and interim storage; high-level waste is stored for 100 years in the so-called HABOG facility.

Discussions between NRG and COVRA have made clear that actinide-bearing fluoride salts are not acceptable for storage in the HABOG facility on account of chemical instability in the presence of water, corrosive action of the salt and radiolytic gas production. Other than these chemical aspects, the burn-up of the samples is relatively low (<1.8 FIHMA) and the tritium content is low as well; actinide weights (Th, U, Pu) are also not higher than for most cases of historic fuel waste. Therefore no SALIENT-specific issues are foreseen related to activity, dose rate and/or decay heat.

NRG has started R&D on conversion of the salts to acceptable waste forms. The initial goal was to use aqueous chemistry to separate the fluorine from the cations to produce high-level oxide waste plus intermediate level cemented liquid waste; the fluorine may then be captured by calcium as  $\text{CaF}_2$  or in the form of fluor-apatite as part of the cemented waste fraction. A particular advantage of aqueous processing is that it can be executed without major changes to hot cell infrastructure, but a strong disadvantage is that significantly more waste is generated from small initial waste volumes. For this reason direct oxidation of the salt with  $\text{B}_2\text{O}_3(\text{s})$ ,  $\text{SiO}_2(\text{s})$  and phosphates (Riley et al., 2019, 2020) is currently being tested, also with a view to treating larger salt volumes in the future.

Interim storage of fluoride salts at NRG will be realized using a gas tight nickel alloy lined steel cask filled with nitrogen and suitable getter materials. Ni-201 and Inconel 600 are corrosion resistant, form a passivating layer with the reactive species  $\text{F}_2(\text{g})$ , and have good  $\text{HF}(\text{g})$ -compatibility (Miki et al., 1990; Corrosion resistance of nickel-containing alloys, 2006). Soda lime or activated nickel may be used to catch radiolytically produced fluorine gas (Brynstad and Williams, 1999). To avoid possible accumulation of  $\text{UF}_6$  formed by the reaction of  $\text{UF}_4(\text{s})$  with  $\text{F}_2(\text{g})$ , the fluoride scavenger  $\text{NaF}(\text{s})$  could be added to the

container in excess.  $\text{NaF}(\text{s})$  reacts with  $\text{UF}_6(\text{g})$  to form the solid  $\text{Na}_2\text{UF}_8(\text{s})$  (Rudolph, et al., 1997; Peretz, 1996; Katz, 1963). However, due to the low concentration of  $\text{UF}_4$  in the LiF-Th $\text{F}_4$  salt, the production of  $\text{UF}_6$  is unlikely to be of concern.

## 6. Discussion

The irradiation of SALIENT-01 proceeded predictably and was completed successfully and without incident. Final crucible wall temperature distributions were well within targets, even when sample power increased by a factor 4 during irradiation. The main limitations of the experiment are therefore not in the irradiation but in the design. The design limitations are briefly discussed here, together with proposed remedies when appropriate.

- The use of graphite crucibles has led to contamination of the salt samples with (in principle inert) amorphous graphite, as concluded from SEM/EDS and XRD measurements. Some fouling of the salt by moderator graphite cannot be avoided in MSRs, but perhaps the application of a ‘cleaning salt’ in the primary system before loading with the fuel salt can help reduce this issue.
- Inspection of similar samples by SEM/WDS revealed the presence of oxygen, which may be residual oxide trapped within the fuel sample or the crucible. The latter is highly unlikely, since the graphite crucibles were heated to 1000 °C, which would have turned all residual oxygen to  $\text{CO}_x(\text{g})$ .
- The use of open crucibles means that salt samples are vulnerable to outside influence during fabrication and assembly. Therefore welded capsules will be used in a follow-up irradiation (SALIENT-03), which will focus on in-pile corrosion of Hastelloy N.
- Since a major intended output of the series of SALIENT irradiations is the screening of fission product stability in fluoride salts at burn-up, the experiment would benefit significantly from sample enrichment with fissile isotopes (enriched U or Pu); this will be done in SALIENT-03.
- Thermocouple placement was not ideal. From CFD analysis, the main temperature gradient in the crucible walls is axial (vertical), and information on this temperature gradient yields information on the salt flow characteristics, which is especially important due to the fact that thermo-physical properties of the salts are often not available. Ideally, thermocouples are placed not only at different axial positions around the salt column but also at the axial center.
- Since uranium fission generates a net surplus of fluorine atoms (very roughly represented by the reaction  $\text{UF}_4 \rightarrow \text{LnF}_3 + \text{M} + \text{F}$ , where Ln represents the lanthanides and M the noble metals) the redox potential of the fluoride salt increases and is therefore ill-defined. This issue of not being able to reliably estimate the redox state of the salt, can be remedied by establishing a ratio  $\text{UF}_4/\text{UF}_3$  of around 10–100, and then evaluating the post-irradiation value of the ratio  $\text{UF}_4/\text{UF}_3$  by a combination of burn-up analysis and thermochemical analysis.
- Perhaps most importantly, lack of heaters means that radiolytic production of  $\text{F}_2(\text{g})$  during reactor downtime cannot be excluded. Although direct effects of  $\text{F}_2(\text{g})$  production were not observed during irradiation, even mild radiolysis would reduce the chemical state of the salt samples significantly, which in turn may have resulted in unwanted interaction with the graphite. This problem can be prevented by installing heaters in the sample holder, which are then used during the shutdown periods. This was already done previously at ORNL (Grimes, 1964, 1965) and MIT (Carpenter et al., 2017).

We finally add that capsule irradiations like SALIENT-01 can provide an environment closely matching the environment of the primary system of MSRs, reproducing temperature, temperature differences in the system and the associated corrosion profiles, salt flow, and the build-up of fission products. Note that the burn-up rate at representative power density is much faster for capsule irradiations than for pumped loops, for

which much of the salt is outside the core. The only direct limitations in this respect are the relatively low salt flow of around 1 cm/s, similar to that of the free convection loops used for laboratory corrosion testing, and the relatively fast build-up of corrosion products such as  $\text{CrF}_x$  in the salt due to low volume to area ratio, which may or may not influence the corrosion rate. Pumped salt loops with heat exchangers would have to be installed in material test reactors to address these last two limitations.

### CRedit authorship contribution statement

**P.R. Hania:** Conceptualization, Investigation, Visualization, Writing - original draft, Writing - review & editing. **D.A. Boomstra:** Methodology, Validation. **O. Benes:** Project administration, Investigation, Visualization, Writing - original draft. **P. Soucek:** Methodology, Validation. **A.J. de Koning:** Methodology, Validation. **I. Bobeldijk:** Project administration. **S. de Groot:** Conceptualization. **R.J.M. Konings:** Supervision, Resources. **E. Capelli:** Methodology, Validation. **M. Naji:** Methodology, Validation. **C. Sciolla:** Software. **P.J. Baas:** Software. **V. Bhimanadam:** Software. **N.B. Siccama:** Software. **G.I.A. Lippens:** Methodology, Validation.

### Declaration of Competing Interest

The authors declare that they have no known competing financial interests or personal relationships that could have appeared to influence the work reported in this paper.

### Acknowledgements

This work was funded by the Dutch Ministry of Economic Affairs and the European Commission. RH would like to thank Luke Olson (Univ. Wisconsin-Madison, currently Westinghouse), David Holcomb (ORNL) and Victor Ignatiev (Kurchatov Institute) for discussions on fluorine generation and corrosion issues.

### Appendix. Impact of $\text{F}_2$ production

#### The ORNL MTR-47 capsule irradiation series

During the design phase for the SALIENT irradiations, much has been learned from similar molten salt capsule irradiations performed at ORNL in the 1960s. In particular, annual progress reports of ORNLs chemistry division (refs (Grimes, 1963c, 1963b, 1964, 1965)) give an interesting account of the MTR-47 capsule irradiations performed in the MTR reactor in the period 1962–1965 as preparation for the MSRE 7–8 MW<sub>th</sub> reactor experiment. Here we give a short summary of the findings presented in those reports.

Following correction of some design flaws in the MTR-47-1 and -2 experiments, the MTR-47-3 design consisted of welded INOR-8 (Hastelloy N) capsules containing a graphite half-shell in contact with MSRE salt ( $65\text{LiF}\cdot 29\text{BeF}_2\cdot 5\text{ZrF}_4\cdot 0.66\text{UF}_4$ ) (Grimes, 1963b; Brandon and Conlin, 1964). During post-irradiation examination it appeared that some salt had moved into the graphite-capsule gap, an indication of in-pile evaporation-condensation which seems to be a particular concern for salts containing  $\text{ZrF}_4$  (Williams et al., 2006). Another unexpected finding was the presence of  $\text{CF}_4$  gas. This prompted a series of ( $\alpha/\beta/\gamma$ ) beam irradiations revealing the radiolytic formation of fluorine ( $\text{F}_2$ ) gas at near room temperature. Apparently the gaseous  $\text{F}_2$  had formed during reactor stops after the samples had cooled down. This gas subsequently reacted with the graphite when temperatures increased during reactor start-up. Post-irradiation analysis also revealed the formation of xenon fluorides ( $\text{XeF}_2$  and  $\text{XeF}_4$ ).

Subsequent experiments MTR-47-4 and -5 (Grimes, 1963a, 1963b, 1964, 1965; Brandon and Conlin, 1964) focused on quantifying fluorine and  $\text{CF}_4$  generation and confirming the compatibility of graphite and INOR-8 with MSRE salt. In a MTR-47-4 capsule where a significant

amount of  $\text{F}_2$  was generated, the  $\text{F}_2$ -exposed graphite surfaces were found to be severely corroded. MTR-47-5 included in-pile pressure measurements, which showed that no gas was formed during low-power operation (at sample temperatures above 88 °C), and that negligible amounts of  $\text{CF}_4$  were formed when the graphite was fully submerged in salt. For flushed capsules which had lost significant amounts of  $\text{F}_2(\text{g})$ , formation of an interaction layer was observed at the interface between the graphite and the strongly reduced fuel salt. The reaction  $4\text{UF}_3 + 2\text{C} \rightarrow 3\text{UF}_4 + \text{UC}_2$  was postulated after observation of  $\text{UC}_2$  in this interaction layer.

Following the conclusion that radiolysis is suppressed at elevated temperature, experiment MTR-47-6 (Grimes, 1965) was designed with electric heater elements to prevent the low-temperature formation of fluorine gas during reactor stops. This experiment provided proof that the observed side reactions were all related to deviations from thermochemical equilibrium caused by low-temperature radiolytic  $\text{F}_2$  production, and that the material system INOR-8 – MSRE salt – CGB graphite is chemically compatible under irradiation in absence of those side reactions. Deposition of uranium in graphite was indeed reduced by a factor 100 compared to MTR-47-5 observations, to a level of 10 ppm.

#### $\text{F}_2$ production rate for SALIENT-01

Williams et al. specify a ‘best estimate’ production efficiency (G-value) of 0.02 molecules  $\text{F}_2$  per 100 eV absorbed energy based on the different irradiation experiments performed up to that time, as well as a maximum G-value of 0.045 molecules  $\text{F}_2/100$  eV. However, especially in salt samples that underwent a melting/solidification cycle the release of fluorine gas is delayed significantly with respect to the start of irradiation. For instance, the MTR-47-5 capsule irradiation by ORNL showed no sign of  $\text{F}_2(\text{g})$  production from MSRE salt during the first 5–10 days following reactor shutdown (Grimes, 1965). This delay may well be related to the diffusive movement of fluorine atoms to grain surfaces, in which case it should be absent for fine-grained samples.

The above discussion already suggests that prolonged irradiation of fluoride salts eventually establishes an equilibrium between the (forward) radiolysis and (reverse) recombination reactions when sufficient concentration of fluorine vacancies has been built up. The 1986 gamma irradiation of MSRE salt by Toth and Felker, using spent fuel from the Oak Ridge material test reactor HFIR as a gamma source, indicated the establishment of such an equilibrium at around a fluorine loss of around 2 mol-% at a temperature of 30–50 °C and a gamma field of 200–500 kGy (Toth and Felker, 1990; Williams et al., 1996).

Information from the MTR-47-4 and MTR-47-5 capsule irradiation tests can provide an alternative estimate of maximum radiolytic fluorine production<sup>2</sup>. Such an estimate may be more relevant to SALIENT-01 irradiation experiment since information from the MTR-47 experiments relates to solidified salts at burn-up. For both irradiation tests, data on fluorine production obtained after several months of post-

<sup>2</sup> Interpretation of the MTR-47 irradiation results is complicated for two main reasons. First, the power densities indicated for the two salt samples in MTR-47–5 (Fig. 8) are average values, while the power density in the final cycle was ‘approximately twice the design value’ Ref.<sup>29</sup>, page 21; power during the last irradiation cycle dominates the decay heat in the first weeks following shutdown. Second, the above interpretation neglects many possible additional influences such as grain size and chemical state of the salt (burn-up, redox potential). It is for instance mentioned in the context of the MTR-47 irradiations that ‘the production of  $\text{F}_2$  ... generally increases with the quantity of uranium burn-up’ (Ref.<sup>28</sup>, page 23). This last claim seems unlikely, since no irradiation damage is accumulated in the salt during irradiation due to its liquid state, and because of the low concentration of fission products. A reasonable estimate for a maximum effect of burn-up may be given by assuming the loss of one fluorine atom per fission according to  $\text{UF}_4 \rightarrow \text{fission} \rightarrow \text{LaF}_3 + \text{M} + \frac{1}{2}\text{F}_2$ . At burn-ups of a few percent FIHMA this assumption yields an additional production of  $\text{F}_2(\text{g})$  <20% of the original estimate.

irradiation cooling time could be related to in-pile power density (Fig. 8). The figure suggests a linear relation between in-pile salt power density and post-irradiation fluorine production, with a slope of 3.2 mol-% loss of  $F_2$  per 100 W/cc in-core power. This is not surprising considering the roughly linear correlation between in-pile power density and post-irradiation decay heat, and the linear relation between absorbed dose and amount of generated  $F_2(g)$ . Assuming that the results presented in Fig. 8 for MSRE salt (LiF-BeF<sub>2</sub>-ZrF<sub>4</sub>-UF<sub>4</sub>) are applicable as well to the salt (LiF-ThF<sub>4</sub>) used in the SALIENT-01 experiment, and given that the end-of-irradiation power density in the SALIENT-01 experiment of  $\leq 150 \text{ W/cm}^3$  (Fig. 5), a maximum fluorine loss from the samples of 4.8 mol-% may be expected.

The discussion given here should of course be taken as an order-of-magnitude estimate, given the many complicating factors: differences in salt composition and density, the different decay chains of U-233 and U-235, grain size dependence of the diffusion processes etc.

### Corrosion of the graphite crucible

The graphite crucibles are in principle well compatible with the salt itself. Interaction of  $F_2(g)$  with graphite is known to proceed above  $\sim 300 \text{ }^\circ\text{C}$ , producing a mixture of  $(CF)_n$  and  $(C_2F)_n$  intercalation compounds, indicated in the following as  $CF_x$ ;  $x$  in  $CF_x$  increases with reaction temperature, from  $\sim 0.5$  at below  $400 \text{ }^\circ\text{C}$  to  $\sim 1$  at above  $550\text{--}600 \text{ }^\circ\text{C}$  (Watanabe and Touhara, 1988; Nazarov et al., 2006; Sato et al., 2001; Watanabe et al., 1980). Decomposition of  $CF_x$  is exothermic, and mostly so for compositions with  $x \sim 1$  formed at high temperature:  $4C_xF \rightarrow CF_4 + (4x - 1)C$ . This decomposition takes place at temperatures above  $500\text{--}600 \text{ }^\circ\text{C}$  (Grimes, 1963b, 1964; Nazarov et al., 2006; Watanabe et al., 1980). In terms of gas formation, a conversion of  $F_2$  to  $CF_4$  reduces pressure by a factor 2 and at the same time reduces the corrosivity towards the containment ( $CF_4$  is a less reactive gas than  $F_2$ ).  $CF_4$  production can therefore be considered safe compared to the situation where all  $F_2$  remains available to react with the steel containment.

Besides the production of  $CF_4$  gas, energy may be stored temporarily in the graphite in the form of  $C_xF$ . In terms of energy stored, a worst case can be described as follows: The fluorine gas formed during a stop reacts with the graphite at high temperature ( $500\text{--}600 \text{ }^\circ\text{C}$ ), forming  $CF_x$  with  $x \sim 1$ . Sudden and full decomposition of  $CF_x$  takes place (f.i. after a short temperature excursion), freeing all stored energy at once. The heat liberated in this scenario can be estimated using the enthalpy of combustion of  $(CF)$ , determined as  $-736 \text{ kJ/mol}$  (Wood et al., 1969). The maximum amount of  $CF$  formed originates from 4.8 mol-% of the fluorine in the salt samples. For SALIENT-01 this amount is 0.024 mol of  $(CF)$  per capsule. Maximum released energy is therefore 18 kJ. Since the heat capacity of graphite is  $\sim 10 \text{ J/molK}$ , the maximum temperature increase in the graphite is  $94 \text{ }^\circ\text{C}$  for 5 crucibles of 60 g (5 mol) each. A sudden but temporary temperature increase of  $94 \text{ }^\circ\text{C}$  for the graphite crucibles would trigger a high temperature alarm (set at  $25 \text{ }^\circ\text{C}$  above operating temperature). In addition, because the temperature ranges of formation and decomposition of the  $CF_x$  with  $x \sim 1$  strongly overlap and the operating temperature of the crucible is above the threshold for decomposition to  $CF_4$  (at around  $610 \text{ }^\circ\text{C}$ ), total stored energy is likely to be significantly lower than the calculated maximum value. Considering the Carbon:  $F_2$  molar ratio of  $\sim 1500:1$  and the thickness of the crucible walls, corrosion of the outer surface of the graphite crucibles is considered a minor effect in the SALIENT-01 irradiation.

### Corrosion of the containment

Because the containment of SALIENT-01 experiment is closed by welding, and before closure is dried and flushed with dry gas at a temperature of  $120 \text{ }^\circ\text{C}$ , the presence of moisture and therefore the formation of  $HF(g)$  as well as effective galvanic pathways are minimized in the plenum of the 1st containment. No significant reaction between dry  $F_2(g)$  and the stainless steel sample holder and thermocouple sheathing

is expected at room temperature.

Any major attack of the containment by fluorine gas would therefore occur during and following reactor start-up, when temperatures return to nominal. Stainless steels are rapidly corroded by fluorine gas above a threshold temperature of  $200\text{--}300 \text{ }^\circ\text{C}$  (Corrosion resistance of nickel-containing alloys, 2006), significantly below the nominal operating temperatures for SALIENT-01 irradiation. Above the threshold temperature, the metal fluoride layer formed by the reaction with  $F_2(g)$  becomes mechanically unstable, so that no passivating layer forms and corrosion may progressively occur.

Therefore the corrosion of the first containment after reactor start-up is limited by the availability of fluorine. Even if all available fluorine reacts with the sample holder, the steel is present in excess by a factor  $> 200$ . Therefore uniform corrosion would produce a corrosion depth  $< 5 \mu\text{m}$ , which would not affect integrity or functionality of the containment. It is concluded that due to the limited availability of fluorine gas, corrosion is unlikely to lead to containment failure; The event of 1st containment failure is also covered by the monitoring of pressure and activity in the 2nd containment.

### References

- Alekseev, P. & Shimkevich, A.L., 2016. On Electrochemical Maintaining of the Given Quality of Molten Salt Reactors. *Int. J. Nucl. Energy Sci. Technol.* 5, 1000163(1–7).
- ASME Boiler and Pressure Vessel Code, Section II, Part D Properties (Metric), Materials. (The American Society of Mechanical Engineers, 2010).
- Beneš, O., Konings, R.J.M., 2012. 3.13 - Molten salt reactor fuel and coolant. In: *Comprehensive Nuclear Materials*. Elsevier, pp. 359–389. <https://doi.org/10.1016/B978-0-08-056033-5.00062-8>.
- Beneš, O., Konings, R.J.M., 2013. Thermochemistry of molten salt reactor fuels. *Proc. Conf. Molten Salts Nucl. Technol.*
- Brandon, C. A. & Conlin, J. A., 1964. MSRE capsule irradiation experiment. <https://digital.library.unt.edu/ark:/67531/metadc871765/> DOI:10.2172/4090371.
- Brynestad, J. & Williams, D. F., 1999. Evaluation of Fluorine-Trapping Agents for Use During Storage of the MSRE Fuel Salt. [http://inis.iaea.org/Search/search.aspx?orig\\_q=RN:32065801](http://inis.iaea.org/Search/search.aspx?orig_q=RN:32065801).
- Carpenter, D., Ames, M., Zheng, G., Kohse, G., Hu, L., 2017. Tritium production and partitioning from the irradiation of lithium-beryllium fluoride salt. *Fusion Sci. Technol.* 71, 549–554.
- Corrosion resistance of nickel-containing alloys in hydrofluoric acid, hydrogen fluoride and fluorine. (2006).
- Forsberg, C.W., Carpenter, D.M., Whyte, D.G., Scarlat, R., Wei, L., 2017. Tritium control and capture in salt-cooled fission and fusion reactors. *Fusion Sci. Technol.* 71, 584–589.
- Forsberg, C., Peterson, P.F., 2015. Spent nuclear fuel and graphite management for salt-cooled reactors: storage, safeguards, and repository disposal. *Nucl. Technol.* 191, 113–121.
- Gibilaro, M., Massot, L., Chamelot, P., 2015. A way to limit the corrosion in the Molten Salt Reactor concept: the salt redox potential control. *Electrochim. Acta* 160, 209–213.
- Grimes, W. R., 1963. Radiation chemistry of MSR system.
- Grimes, W. R., 1963. Reactor Chemistry Division annual progress report for period ending January 31.
- Grimes, W. R., 1963. Reactor Chemistry Division annual progress report for period ending January 31, 1962.
- Grimes, W. R., 1964. Reactor Chemistry Division annual progress report for period ending January 31.
- Grimes, W. R., 1965. Reactor Chemistry Division annual progress report for period ending January 31.
- Haubenreich, P. N., 1970. Fluorine production and recombination in frozen MSR salts after reactor operation. [http://inis.iaea.org/Search/search.aspx?orig\\_q=RN:2006386](http://inis.iaea.org/Search/search.aspx?orig_q=RN:2006386).
- Heijna, M.C.R., de Groot, S., Vreeling, J.A., 2017. Comparison of irradiation behaviour of HTR graphite grades. *J. Nucl. Mater.* 492, 148–156.
- Katz, S., 1963. Apparatus for the gasometric study of solid-gas reactions: sodium fluoride with hydrogen fluoride and uranium hexafluoride. <https://catalog.hathitrust.org/Record/007842258>.
- Kelleher, B. C., 2015. Purification and Chemical Control of Molten Li<sub>2</sub>BeF<sub>4</sub> for a Fluoride Salt Cooled Reactor.
- LeBlanc, D., 2010. Molten salt reactors: a new beginning for an old idea. *Nucl. Eng. Des.* 240, 1644–1656.
- MCNP-A general Monte Carlo N-particle transport code. Version 4C. (2000).
- Merle, E., Heuer, D., Allibert, M., Ghetta, V. & Le Brun, C., 2008. Introduction to the Physics of Molten Salt Reactors. DOI:10.1007/978-1-4020-8422-5.25.
- Miki, N., Maeno, M., Maruhashi, K., Nakagawa, Y., Ohmi, T., 1990. Fluorine passivation of metal surface for self-cleaning semiconductor equipment. *IEEE Trans. Semicond. Manuf.* 3, 1–11.

- Nazarov, A.S., Makotchenko, V., Fedorov, V.E., 2006. Preparation of low-temperature graphite fluorides through decomposition of fluorinated-graphite intercalation compounds. *Russ. J. Inorg. Mater.* 42, 1260–1264.
- Olson, L.C., 2009. *Materials Corrosion in Molten LiF-NaF-KF Eutectic Salt*. University of Wisconsin-Madison.
- Peretz, F. J., 1996. Identification and evaluation of alternatives for the disposition of fluoride fuel and flush salts from the molten salt reactor experiment at Oak Ridge National Laboratory, Oak Ridge, Tennessee. [http://inis.iaea.org/Search/search.aspx?orig\\_q=RN:28076712](http://inis.iaea.org/Search/search.aspx?orig_q=RN:28076712).
- Riley, B.J., et al., 2019. Molten salt reactor waste and effluent management strategies: a review. *Nucl. Eng. Des.* 345, 94–109.
- Riley, B.J., Peterson, J.A., Vienna, J.D., Ebert, W.L., Frank, S.M., 2020. Dehalogenation of electrochemical processing salt simulants with ammonium phosphates and immobilization of salt cations in an iron phosphate glass waste form. *J. Nucl. Mater.* 529, 151949.
- Robertson, R. C., 1791. Conceptual design study of a single-fluid molten salt breeder reactor. Other Information: UNCL. Orig. Receipt Date: 31-DEC-71 <https://digital.library.unt.edu/ark:/67531/metadc867701/> DOI:10.2172/4030941.
- Rosenthal, M. W., 1972. Development status of molten salt breeder reactors. <https://www.osti.gov/biblio/4622532-development-status-molten-salt-breeder-reactors> DOI:10.2172/4622532.
- Rudolph, J. C. et al., 1997. Laboratory tests in support of the MSRE reactive gas removal system.
- Sabharwall, P., Ebner, M., Sohal, M., 2010. *Molten Salts for High Temperature Reactors: University of Wisconsin Molten Salt Corrosion and Flow Loop Experiments – Issues Identified and Path Forward*. Office of Nuclear Energy, Science, and Technology, United States.
- Sato, Y., Hagiwara, R., Ito, Y., 2001. Thermal decomposition of 1st stage fluorine-graphite intercalation compounds. *J. Fluor. Chem.* 110, 31–36.
- Serp, J. et al., 2014. The molten salt reactor (MSR) in generation IV: Overview and perspectives. vol. 77.
- Souček, P., et al., 2017. Synthesis of UF<sub>4</sub> and ThF<sub>4</sub> by HF gas fluorination and re-determination of the UF<sub>4</sub> melting point. *J. Fluor. Chem.* 200, 33–40.
- Stempniewicz, M. M. et al., 2017. Design and safety support analyses of an in-pile molten salt loop in the HFR with the SPECTRA code.
- Taira, M., Arita, Y., Yamawaki, M., 2017. The evaporation behavior of volatile fission products in FLiNaK Salt. *Open Access J. Sci. Technol.* 5.
- Toth, L. M. & Gilpatrick, L. O., 1972. The equilibrium of dilute UF<sub>3</sub> solutions contained in graphite.
- Toth, L.M., Felker, L.K., 1990. Fluorine generation by gamma radiolysis of a fluoride salt mixture. *Radiat. Eff. Defects Solids* 112, 201–210.
- Vreeling, J. A., Wouters, O. & van der Laan, J. G., 2008. Graphite irradiation testing for HTR technology at the High Flux Reactor in Petten. *J. Nucl. Mater.* 381, 68–75.
- Watanabe, Nakajima, T. & Touhara, H., 1988. *Graphite Fluorides*, Volume 8 - 1st Edition. (Elsevier).
- Watanabe, N., Koyama, S., Imoto, H., 1980. Thermal decomposition of graphite fluoride. I. Decomposition products of graphite fluoride, (CF)<sub>n</sub> in a vacuum. *Bull. Chem. Soc. Jpn.* 53, 2731–2734.
- Williams, D. F., Del Cul, G. D. & Toth, L. M., 1996. A descriptive model of the molten salt reactor experiment after shutdown: Review of FY 1995 progress. <https://digital.library.unt.edu/ark:/67531/metadc664872/> DOI:10.2172/230260.
- Williams, F., D., M. Toth, L. & Clarno, K., 2006. Assessment of Candidate Molten Salt Coolants for the Advanced High Temperature Reactor (AHTR).
- Wood, J.L., Badachhane, R.B., Lagow, R.J., Margrave, J.L., 1969. Heat of formation of poly(carbon monofluoride). *J. Phys. Chem.* 73, 3139–3142.
- Zheng, G., He, L., Carpenter, D., Sridharan, K., 2016. Corrosion-induced microstructural developments in 316 stainless steel during exposure to molten Li<sub>2</sub>BeF<sub>4</sub>(FLiBe) salt. *J. Nucl. Mater.* 482, 147–155.